13th World Conference on Earthquake Engineering
Vancouver, B.C., Canada
August 1-6, 2004
Paper No. 148

SEISMIC RESPONSE OF HIGH-RISE RC BEARING-WALL STRUCTURES WITH IRREGULARITIES AT BOTTOM STORIES

Han-Seon Lee[1] and Dong-Woo Ko[2]

SUMMARY

Many RC building structures of multiple uses constructed in Korea have the irregularities of torsion and/or soft story at bottom stories. The objective of this study is to investigate through shaking table tests the seismic response of high-rise RC bearing-wall structures with three types of irregularity at the bottom stories. For this purpose, three 1:12 scale 17-story reinforced concrete model structures were constructed according to the similitude law, in which the upper 15 stories have a bearing-wall system while the lower two stories have the frame system with different layouts in plan: The first one has only a moment-resisting frame system (Model 1), the second has an infilled shear wall in the central frame (Model 2), and the third has an infilled shear wall in only one of the exterior frames (Model 3). Then, these models were subjected to the same series of simulated earthquake excitations.

The test results show the followings: 1) The existence of shear wall reduces remarkably shear deformation at the lower frame, but has almost a negligible effect on the reduction of the overturning deformation, base shear, and overturning moment (OTM). 2) As the earthquake intensity increases, the structures with symmetric plan experienced the shift of rotating axis (rocking behavior) due to OTM. The model with torsional irregularity shows the uni-directional OTM transverse to the direction of excitations. The effects of two orthogonal OTM's and torsional moment complicate the distribution of axial forces in columns, which need further analytical research in the future. And, 3) the value of torsional stiffness varies depending on the governing mode of vibrations. A higher mode of vibration induces larger torsional stiffness. And, hysteretic curve and the strength diagram between base shear and torque clearly reveal the most probable mode of vibration leading to failure.

Keywords: concrete, buildings, shaking table tests, irregularity, overturning moment, torsion

INTRODUCTION

Due to the severe shortage and for the effective use of the sites for new constructions in metropolitan areas in Korea, the buildings of different uses along the height have been built frequently during the past decade. The most common structural system has been the moment-resisting space frame for the lower stories and the bearing-wall system for the upper stories since the lower stories usually accommodate the parking area, commercial space, garden, or just open spaces for the architectural reasons and the higher stories are generally used as apartment. This type of building structures, which are called piloti-type

[1] Professor, Korea University, Seoul 136-701, Korea, Email: hslee@korea.ac.kr
[2] Graduate student, Korea University, Seoul 136-701, Korea

buildings in Korea, usually have the irregularity of weak story and/or torsion since many upper bearing walls discontinue at the lower stories for some architectural reasons.
The objective of the study stated herein is to investigate the seismic performance of three types of high-rise reinforced-concrete (RC) bearing-wall structures having irregularity of weak story and/or torsion at the bottom stories.

MODEL AND EXPERIMENTAL SETUP

From the inventory study on the available buildings using piloti–type structures in Korea [1], three types of 17–story reinforced concrete structure were selected as prototype. These building structures were designed according to the Korean design codes: Design Code for Concrete Structure [2] and Standard design loads for buildings [3].
The reduction scale of the model was determined as 1:12 after considering the capacity of the available shaking table. Three 1:12 scale 17-story reinforced concrete model structures were constructed according to the similitude law [4], in which the upper 15 stories have a bearing-wall system while the lower two stories have the frame system with different layouts in plan: The first one has only a moment-resisting frame system (Model 1) [5], the second has an infilled shear wall in the central frame (Model 2) [6], and the third has an infilled shear wall in only one of the exterior frames (Model 3) as shown in Fig. 1. Since the rigidity of the upper bearing-wall system was considered to be much higher than that of the lower frame system, the upper system was constructed separately from the lower frame system as a rigid

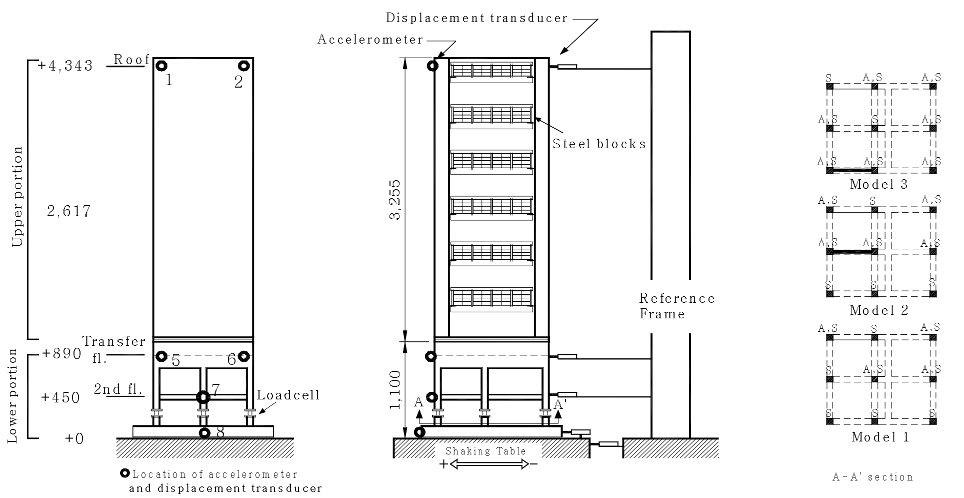

(a) Front view **(b) Side view** **(c) Plan**

Fig. 1 Model and experimental setup (unit: mm)

Table 1 Similitude law [4]

Item	Dimension	True replica model	Modified replica model
Length, l	L	1/12	1/12
Area, A	L^2	1/144	1/144
Mass, M	M	1/144	1/288
Force, F	$ML\,T^{-2}$	1/144	1/144
Acceleration, $\ddot{x}$	LT^{-2}	1	2
Frequency, f	T^{-1}	$\sqrt{12}$	$\sqrt{24}$
Time, t	T	$1/\sqrt{12}$	$1/\sqrt{24}$

concrete box with the steel plates attached as artificial mass. Although the upper bearing-wall structure was modeled as a dummy concrete box, the lower frame was constructed to conform to the requirements for the true replica model in the similitude law, as shown in Table 1 [4], as closely as possible. The dimension of the members and the details of the reinforcements are presented in Fig. 2. However, the limitation in the capacity of the available shaking table caused the total mass of this model to be half the weight required for the true replica model in the similitude law. The applied peak ground acceleration (PGA) had to be twice the PGA required for the true replica model due to the reduction of weight as shown in the second column in Table 1. In this case, the effect of gravity load cannot be fully simulated since only half of the weight required for the true replica model is provided.
The main model reinforcement D2 (2mm diameter) for D25 in prototype was made by deforming the surface of commercially available wires of similar diameter and then annealing by using the vacuum electric furnace. The target in annealing was aimed at obtaining the model reinforcement of the same or similar yield force, rather than yield stress as required by the similitude law, because it was impossible to obtain the wire with the section area conforming exactly to the similitude law. For the model transverse reinforcement corresponding to D13 in prototype, commercially available ϕ1.1(1.1mm diameter) wire was used without deforming and heat treatment. The required nominal yield forces for D2 and ϕ1.1 model reinforcement are 1.34 kN and 0.345 kN, whereas the yield forces obtained from test are 1.74 kN and 0.456 kN, respectively. Therefore, the overstrengths of model yield strengths are 26% and 32% for D2 and ϕ1.1, respectively. The model concrete has a 28-day compressive strength of 34.5Mpa on average. The aggregates for the model concrete were scaled down to 1/12 of those of the prototype. The total weight of the model including the artificial mass was estimated to be 91.3kN.
The elevation and plan of the model, the experimental arrangement, and the instrumentation to measure the displacements, accelerations, forces, and local behaviors are shown schematically in Fig. 1. The drifts and accelerations were measured only in the direction of table excitations. The self-made load cells were installed at the mid-height of all the columns at the first story to measure the shear forces (denoted as S), but axial forces were measured (denoted as A) in only 4 ~ 7 columns out of 9. The reference frame to measure the lateral displacement of the model was established outside the shaking table.
The earthquake simulation tests were performed by using the shaking table at the Korea Institute of Machinery and Materials (KIMM), which is 4m$\times$4m and has 6 degrees of freedom, as shown in Fig. 3. The program of earthquake simulation tests is shown in Table 2. The significance of each earthquake simulation test is briefly explained in the remark column. Before and after each earthquake simulation

Table 2 Test program

Test	PGA (g)		Remark
	Prototype	Model	
Taft011	0.055	0.11	
Taft022	0.11	0.22	Design earthquake ($I_E = 1.0$)
Taft030	0.15	0.3	Design earthquake ($I_E = 1.5$)
Taft040	0.2	0.4	
Taft060	0.3	0.6	
Taft080	0.4	0.8	Design earthquake in a highly seismic region
Taft120	0.6	1.2	Maximum considered earthquake in a highly seismic region

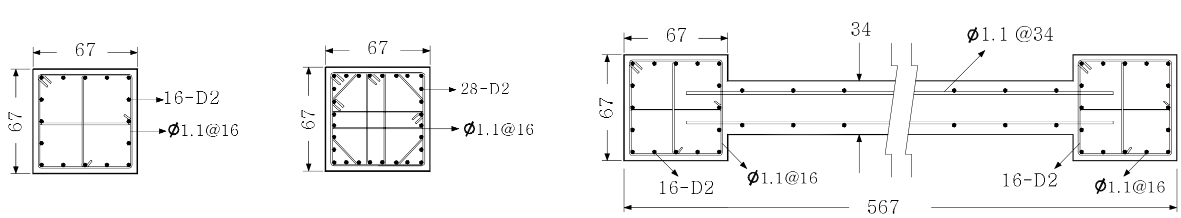

(a) All Columns (b) corner columns of Model 3 (c) Infilled shear wall (Model 2)

Fig. 2 Dimension and reinforcement of members (unit: mm)

test, the white-noise test was conducted to investigate the change in the natural period of the model.

TEST RESULT

The responses of the models under Taft030 and Taft080 will be mainly treated in this paper, since the former is assumed to represent the design earthquake in Korea, and the latter is a typical severe earthquake in highly seismic regions of the world.

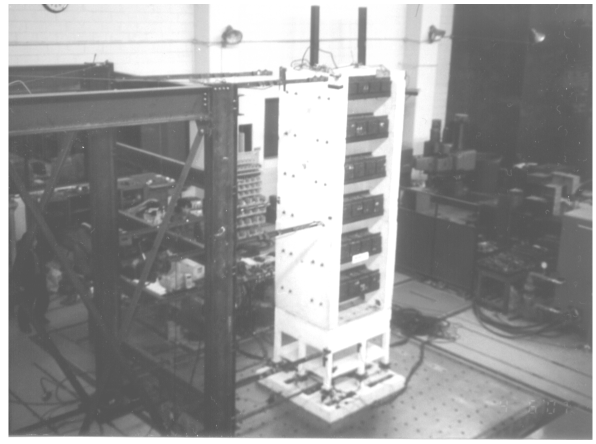

Fig. 3 Overview of the model and experimental arrangement

Changes in dynamic characteristics of models

Fig. 4 shows the change of base shear coefficients and natural periods of each model. The coefficients of base shears under design earthquake (Taft030) appear to be 0.129, 0.128, and 0.135 for Model 1, 2, and 3, respectively, which are over 2.5 times the design coefficient, 0.048. The value of the natural period converted from the calculated period of the prototype structure, 0.920 sec, by the similitude law is 0.188 sec, which is similar to the initial period of 0.193 sec, 0.149 sec, and 0.156 sec for Model 1, 2, and 3, respectively.

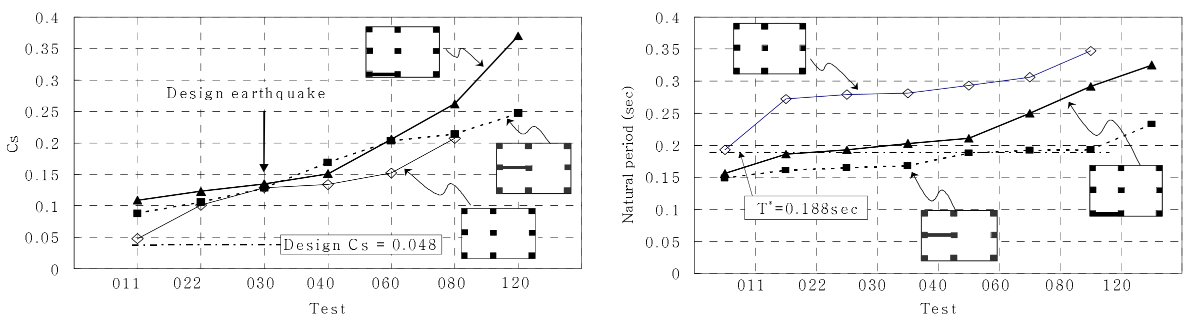

(a) C_s **(b) Natural period**

Fig. 4 C_s and natural period

Global deformations

Because the upper portion of the model is expected to behave almost as a rigid body due to its relatively high rigidity, the global response of the model can be characterized by three kinds of global deformations in the lower frame: shear deformation (θ_1), overturning deformation (θ_2), and torsional deformation (θ_3), whose definitions are shown in Fig. 5. The overturning deformations of the stiff and flexible frames and the torsional deformations at the levels of the roof and transfer floor are compared in Fig. 7 and 8. From this comparison, the upper portion proves to behave almost as a rigid body. However, even with the rigid-body action of the upper portion, the shear deformation in the lower frames can be different depending on the location of the frame such as in Model 3. In Fig. 6, the shear deformations in the stiff and flexible frames in the direction of table excitation are greatly different whereas those in exterior frames in Model 1 and 2 are almost identical.

The shear deformation (θ_1) is about 3.5 times the overturning deformation (θ_2) in case of Model 1. The roof drift due to the shear deformation at piloti stories is approximately half of the total roof drift. Model 2 has similar values for the shear and overturning deformations. Therefore, the overall drift shape appears to be approximately linear in Model 2. While the amount of the shear deformation at piloti stories has been greatly reduced, the overturning deformation remains to be almost same or a little increased when compared with the case of Model 1.

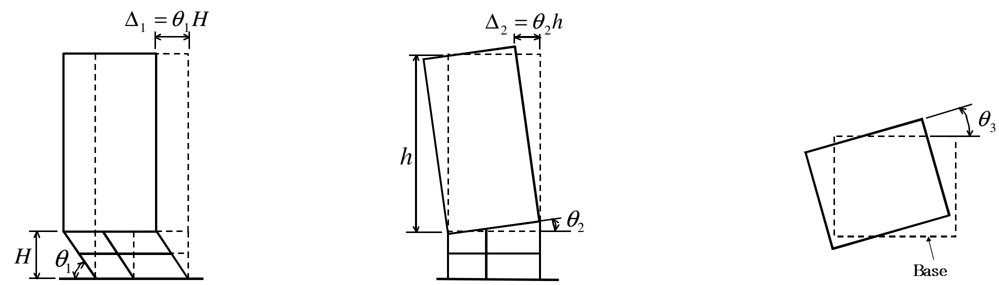

(a) Shear deformation(θ_1) (b) Overturning deformation(θ_2) (c) Torsional deformation(θ_3)

Fig. 5 Definition of shear, overturning and torsional deformations

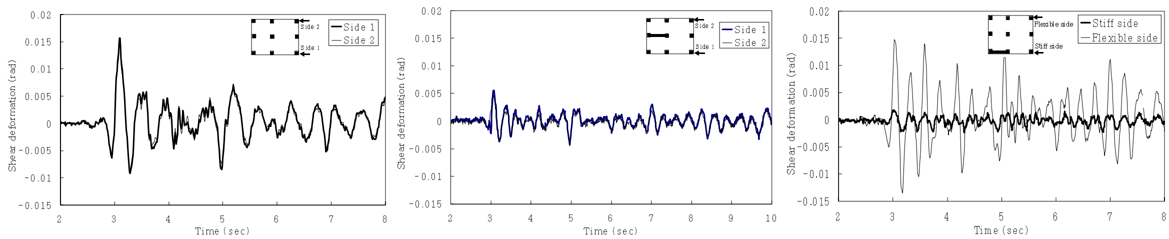

(a) Model 1 (b) Model 2 (c) Model 3

Fig. 6 Shear deformation (Taft080)

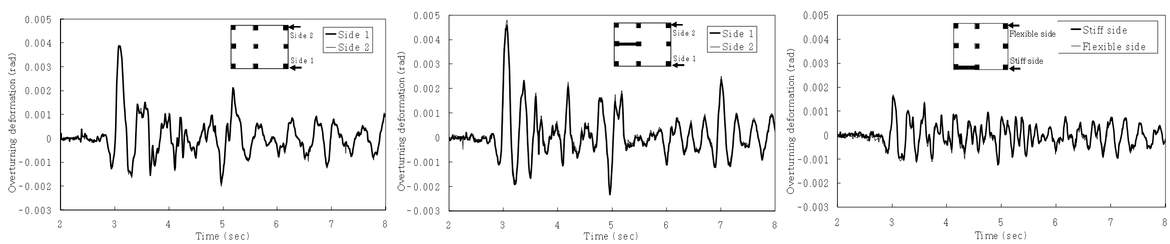

(a) Model 1 (b) Model 2 (c) Model 3

Fig. 7 Overturning deformation (Taft080)

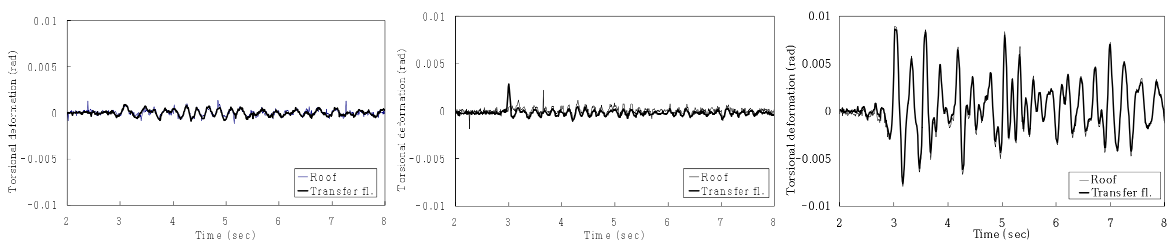

(a) Model 1 (b) Model 2 (c) Model 3

Fig. 8 Torsional deformation (Taft080)

Model 3 shows the behavior of Model 1 for the flexible frame but that of Model 2 for the stiff frame with regards to the shear deformation at piloti stories. However, it is interesting to note that the overturning deformations in the stiff and flexible frames are same and much smaller than those of the Model 1 and 2. The interstory drift indices at the bottom two stories are within 1.5% in all models under Taft080.

Base shear, overturning moment (OTM), and torsional moment

Fig. 9, 10, and 11 show the time histories of the base shear, base OTM, and base torsional moment under Taft080. These were derived from measured accelerations at four corners (No. 1, 2, 5, and 6 in Fig. 1 (a)), by assuming the linear distribution of accelerations between these points and the uniform density of mass over the whole volume of the upper structure. The base shear can be derived from two systems of measurement: That is, (1) by summing the shear forces measured at the load cells installed at the mid-height of the first-story columns and (2) by summing the inertia forces along the height of the model calculated by multiplying the measured acceleration with the corresponding estimated mass. The base shear for each bent of frames without the shear wall was measured directly from the load cells installed at the mid-height of the first-story columns. However, the base shear for the stiff bent, which includes the shear wall, was calculated by subtracting the sum of shears in the bents without shear wall from the total base shear. It can be noted that these two base shears are almost identical in Model 1. In Model 2 and 3, the difference between the value of base shear derived from the load cells and that obtained from inertia forces means the shear resisted by the shear wall including the boundary columns, and amounts to 75% of the base shear in Model 2, but only 30% in Model 3. The maximum values of OTM appear to be similar and the phase of OTM is almost identical with that of base shear in three models.

Torsional moment in Model 1 and 2, derived from the measured accelerations, is shown in Fig. 11. Though Model 1 and 2 are symmetric buildings, torsional moments occurred ranging from –9kN-m to 7kN-m and from –4kN-m to 2kN-m for Model 1 and 2, respectively, as shown in Fig. 11 (a) and (b) excluding some unreliable sharp peaks. It means accidental torsion due to uncertainty on the structural properties.

In case of Model 3, the time history of resisting torsional moment, $M_{T,P}$, contributed by two exterior bents parallel to the direction of earthquake excitation with respect to the center of mass (CM) is superposed with thick line to that of total acting torsional moment (thin line), M_T, derived from the measured accelerations in Fig. 11 (c). The difference between the thin and thick lines shows the torsional moment resisted by the base shears in the bent frames perpendicular to the direction of the earthquake excitations,

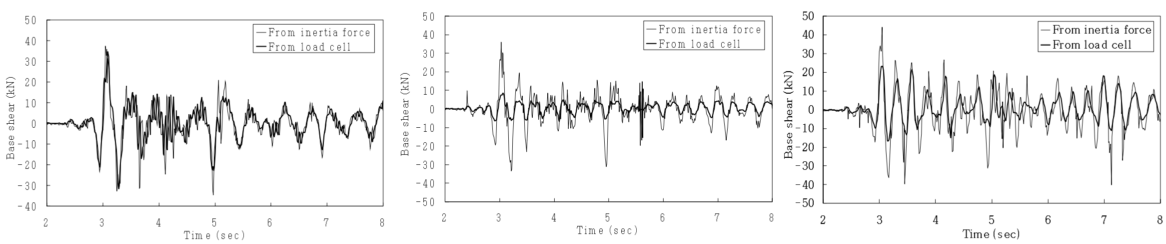

(a) Model 1 **(b) Model 2** **(c) Model 3**

Fig. 9 Time histories of base shear (Taft080)

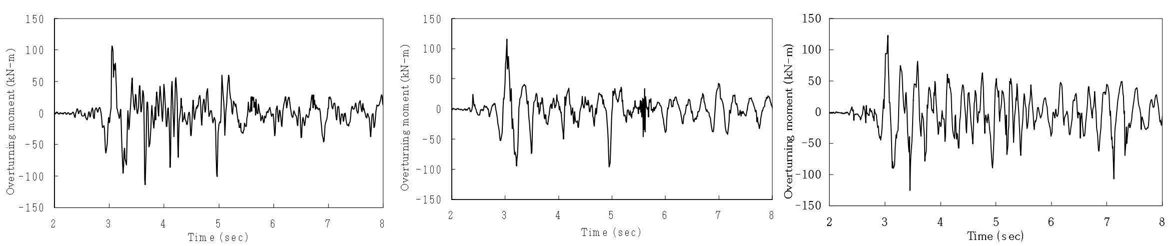

(a) Model 1 **(b) Model 2** **(c) Model 3**

Fig. 10 Time histories of overturning moment (Taft080)

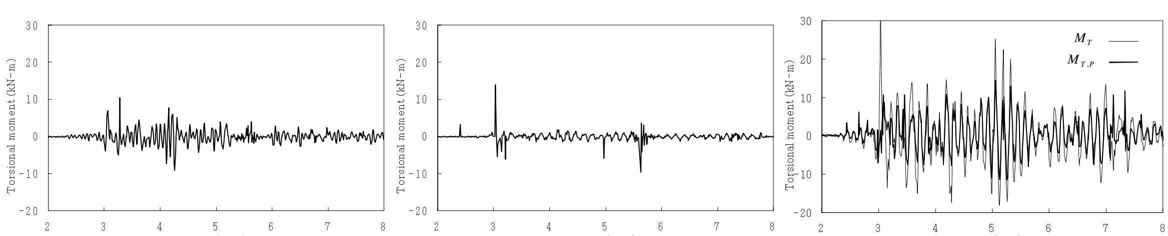

(a) Model 1 **(b) Model 2** **(c) Model 3**

Fig. 11 Time histories of torsional moment (Taft080)

and by the torsional rigidity of the shear wall itself, if any. The contribution of these transverse bent frames to the total torsional resistance appears to be about 30 to 40% under Taft080, which cannot be ignored, even though the transverse bent frames do not include any shear walls.

Relation between base shear and drift at transfer floor

Fig. 12 and 13 depict the hysteretic behaviors between the base shear and the lateral drift at the level of transfer floor under Taft030 and Taft080, respectively. The hysteretic relation for Taft030 appears to be the almost linear elastic, in which the stiffness is 5.96kN/mm, 20.92kN/mm and 11.20kN/mm, respectively for Model 1, 2, and 3. The stiffness of piloti stories of Model 2 is 3.5 times larger than that of Model 1. However, under Taft080 the non-linearity and energy dissipation increased while the stiffness decreased to 62%, 47% and 49%, respectively for Model 1, 2, and 3.

Each point in Fig. 14 means the bent base shear and the drift at the transfer floor at the time of the maximum roof drift for each test. And the curves connecting these points reveal the envelope relation between the bent base shear and drift at the transfer floor. In Model 1 as shown in Fig. 14 (a), the central fame has the stiffness of 3.16kN/mm, which is about 1.7 times those of the exterior frames even if the size and reinforcements of the columns are same in the three bents. However the yielding strength of all bents are similar. From Fig. 14(b), which depicts the case of Model 2, it can be noticed that the drifts are very small when compared with those of Model 1 and that most of the lateral load is resisted by the central frame which contains the shear wall. The strength of the exterior bents seems to be too low when compared with those of Fig. 14(a) and (c). The values of stiffness of the exterior frames are 1/5 and 1/11 times that of the central frame. The central frame containing the shear wall behaves linearly up to Taft060, but displays the yielding under Taft080. In Fig. 14 (c) for Model 3, the stiffness of the stiff exterior frame appears to be 17.05kN/mm and much larger than that of the central frame in Model 2, 12.90kN/mm. In Model 3 the stiff exterior frame containing the shear wall remains elastic even under Taft120 whereas the flexible exterior frame has shown the incipient yielding under Taft040. It is interesting to note that the maximum lateral displacement at the flexible frame of Model 3 is almost equal to that of Model 1 under Taft080. This means that though a structure has a large torsional eccentricity, this does not necessarily lead to a larger displacement to the flexible side of the same structure than that of no eccentricity and same flexibility in all frames such as Model 1.

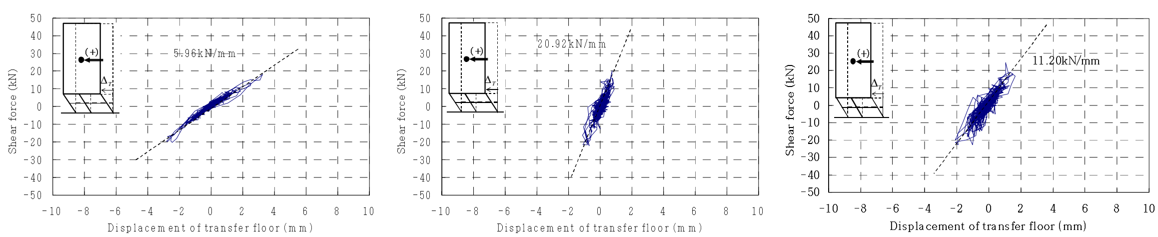

(a) Model 1 **(b) Model 2** **(c) Model 3**

Fig. 12 Relation between base shear and drift at transfer floor (Taft030)

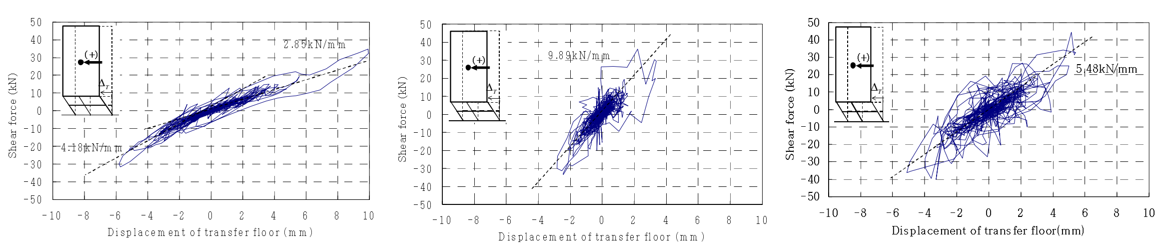

(a) Model 1 **(b) Model 2** **(c) Model 3**

Fig. 13 Relation between base shear and drift at transfer floor (Taft080)

Overturning behavior

Fig. 15 and 16 present the hysteretic relation between the overturning moment (OTM) at the level of the base and the overturning angle at the level of the transfer floor as defined in Fig. 8. The three models

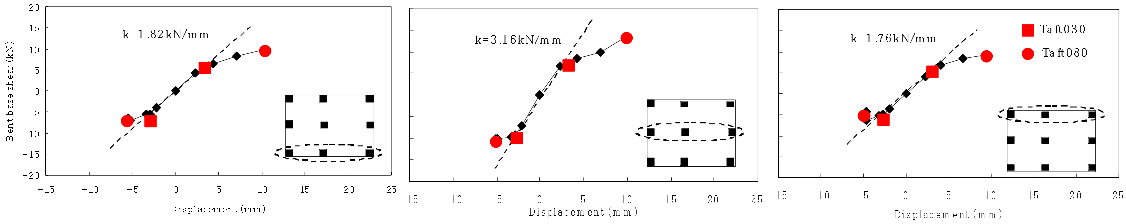

(a) Model 1

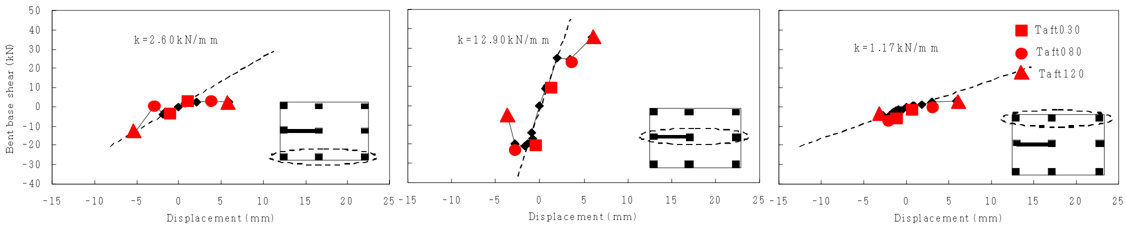

(b) Model 2

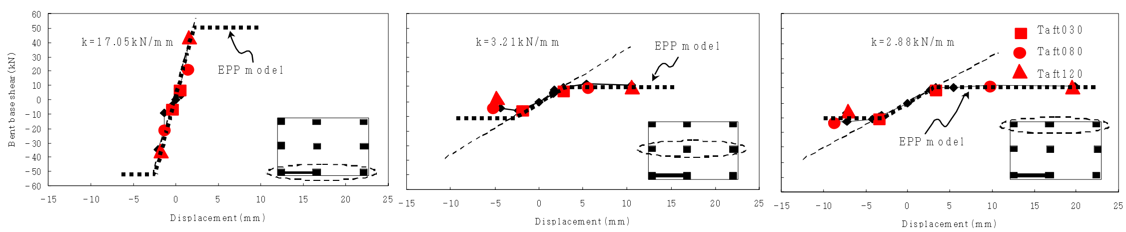

(c) Model 3

Fig. 14 Envelope of bent base shear and displacement at transfer floor

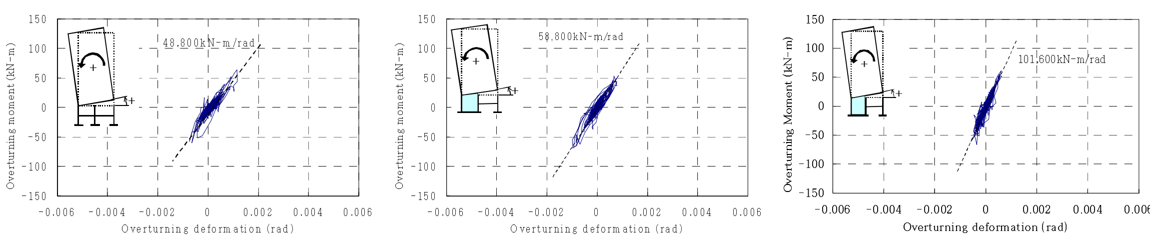

(a) Model 1 **(b) Model 2** **(c) Model 3**

Fig. 15 Relation between overturning moment and deformation (Taft030)

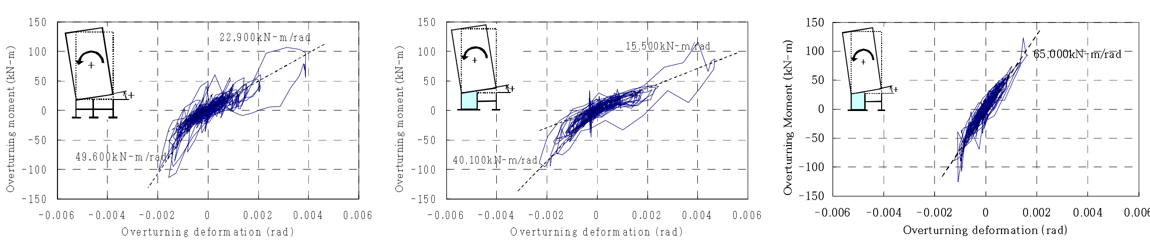

(a) Model 1 **(b) Model 2** **(c) Model 3**

Fig. 16 Relation between overturning moment and deformation (Taft080)

reveal almost linear elastic behavior under test Taft030, but Model 1 and 2 began to show the inelastic behavior and large degradation in stiffness particularly in the positive direction under Taft080. The stiffness has decreased to 47%, 26%, 64% under Taft080, respectively for Model 1, 2, and 3. This larger stiffness degradation in the positive direction than the negative may be attributed to the sudden decrease in the tension stiffness in column. Fig. 17 shows the equilibrium with respect to the OTM which can be expressed by the following equations:

$$M_{OT} + \sum x_i F_i + \sum M_i + M_{OT,W} = 0 \quad (1)$$

$$M_{OT,W} = l \times \sin(\alpha - \theta) \times W \approx l \times \sin\alpha \times W \quad (2)$$

where, W : the weight of structure, F_i, M_i : axial force and flexural moment in vertical element i , x_i : the distance of vertical element i from the axis of rotation, O . Since the rotation, θ , is on the order of 0.001 rad, $M_{OT,W}$ can be approximated by $(l \sin\alpha) \times W$. It should be noted that the location of the axis of rotation, O , in Fig. 17 plays an important role in the resisting OTM and that this location may not be known and fixed throughout the response. The location of the rotational axis, O , can be estimated by investigating the relation between the measured axial force and the axial deformation derived from the overturning deformation, θ .

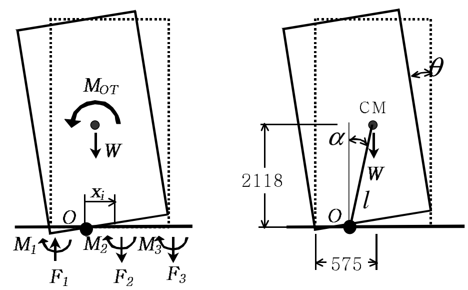

(a) M_{OT} (b) Self weight

Fig. 17 Overturning equilibrium (unit:mm)

Fig. 18 (a) shows the time histories of elongation and shortening of the central column in Model 1 when the rotation axes are assumed to locate at the positions denoted by double-headed arrows. However, the time history of axial force denoted with a thin line in Fig. 18 (b) reveals that only the elongation part in the history in Fig. 18 (a) is effective. This means that the shift of the rotational axis has occurred depending on the direction in overturning and this phenomenon is generally called "rocking behavior."

Using trial-and-error procedures, the locations of the rotational axis were estimated and the results are shown in Table 3. As the intensity of earthquake increases, the range in the shift of rotational axis also generally increases. However, Model 2 did not show any shift under Taft030. The resisting OTM's with the assumption of shifted and fixed rotational axes are shown in Fig. 19. The error with the fixed rotation can be 15% in the negative direction (t = 3.23 sec) and 100% in the positive (t = 3.38 sec) in Model 2. However, the ranges of the resisting OTM are very similar regardless of rocking phenomenon as can be observed in Fig. 19.

With the estimation of the location of rotational axis, the OTM resisted by self weight can be calculated using eq. (2). Time histories of the acting OTM by inertia forces, the resisting OTM due to measured axial forces with consideration of rocking phenomena are shown in Fig. 20. The contribution by the self weight is accumulated to that by the measured axial forces and denoted by a solid mark at some peak points in

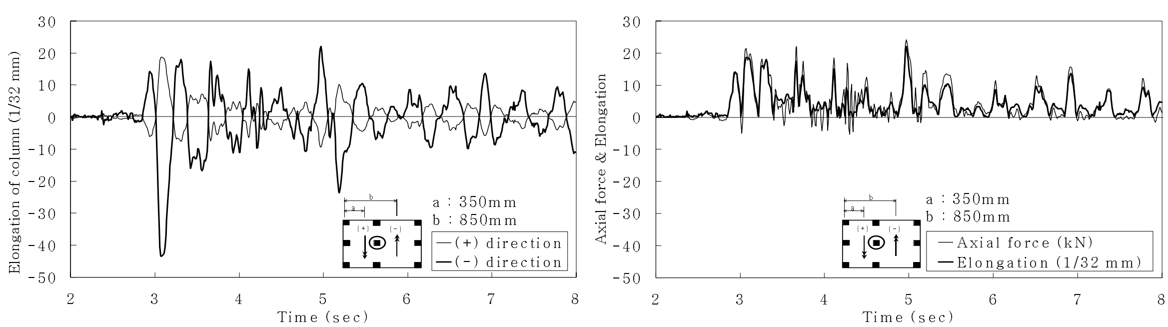

(a) Elongation of column **(b) Elongation and axial force**

Fig. 18 Comparison of elongation and axial force (Model 1: Taft080)

this figure. The portion resisted by the self weight is from zero to 36% of the total acting OTM.
Though the lateral displacements and accelerations in the transverse direction were not measured at all, the resisting OTM's about two orthogonal axes centered at the CM, contributed by instrumented seven columns are shown in Fig. 21 (a) for Taft080. Even if the contributions by non-instrumented two columns and by the panel portion in the shear wall were not included in this derivation, it is apparent in Figure 21 (a) that the amount of OTM in the transverse direction, $M_{OT,T}$, is significant when compared with that in

Table 3 Location of rotational axis (RA) (unit : mm)

Test \ RA \ Model	Model 1		Model 2		
	a	b	a	b	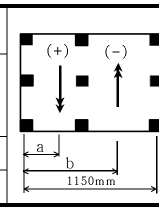
Taft030	450	850	350	350	
Taft080	350	850	250	700	

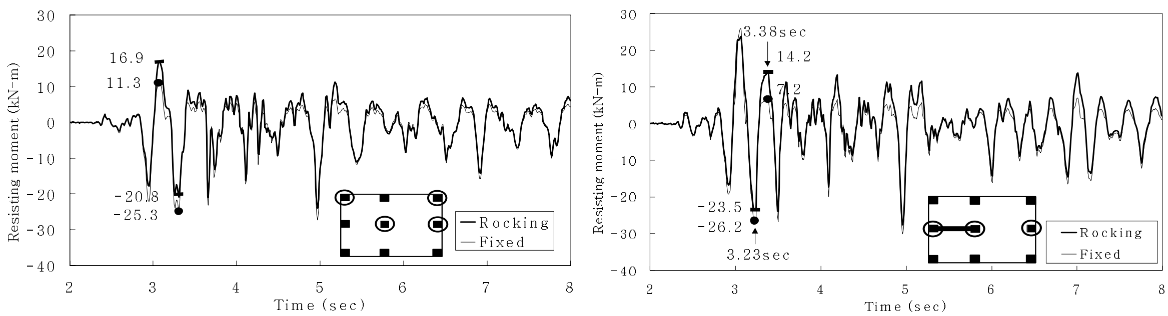

(a) Model 1 **(b) Model 2**

Fig. 19 Time histories of resisting OTM in rocking and fixed rotation (Taft080)

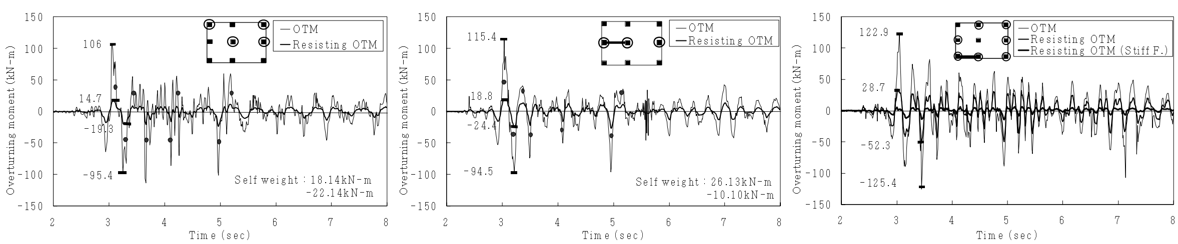

(a) Model 1 **(b) Model 2** **(c) Model 3**

Fig. 20 Comparison of base OTM and resisting OTM

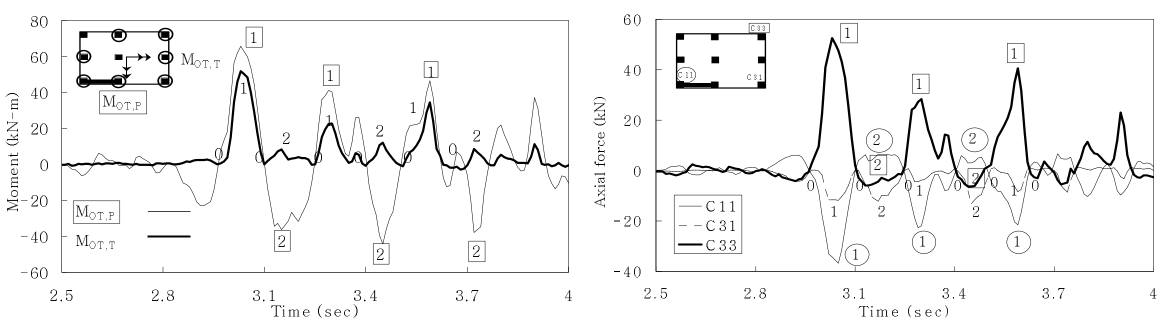

(a) Resisting moment **(b) Axial forces**

Fig. 21 Comparison of OTM's in orthogonal directions and axial forces

the direction of earthquake excitations, $M_{OT,P}$. The $M_{OT,T}$ in experiment is unilateral and has a period approximately the same as one half the period of the $M_{OT,P}$. The time histories of axial forces in three corner columns are given in Fig. 21 (b) to illustrate the relationship with the OTM in Fig. 21 (a), by putting the sign of status, 0, 1, and 2 to the corresponding points. The axial forced in three corner columns show the bias in tension or in compression due to the unilateral OTM in the transverse direction.

Torsional behavior

In Fig. 22 the torsional stiffness during t = 2.0 sec ~ 4.0 sec, when the second mode governs, appears to be approximately 1,200 kN-m/rad under Taft080, and increases to about 4,500 kN-m/rad during t = 4.0 sec ~ 6.0 sec when the third mode became predominant, and then returned to the initial stiffness. In order to illustrate the effect of mode shape on the torsional stiffness, the mass and stiffness matrices for a single-story model with 3 degree of freedom (u_x, u_y, and u_θ) were derived and given in Table 4 with the calculated mode vectors by using the values of the instantaneous shear stiffness for each bent (t = 2.98 sec ~ 3.28 sec for Taft080) and by assuming that the shear stiffness of transverse bents be the same as that of the flexible bents parallel to the direction of excitation. If the viscous damping is ignored and the free vibration assumed, the equation of motion with respect to the torsion can be expressed as follows:

$$1{,}583\ddot{u}_\theta + 8{,}411u_x - 419u_y + 6{,}338{,}747u_\theta = 0 \qquad (3)$$

By using eq. (3) and the vectors of the second and third modes as given in Table 4, the values of torsional stiffness for the second and third modes are obtained and given 1,526 kN-m/rad and 9.144 kN-m/rad, respectively. Though the value of the second mode roughly matches that (1,200 kN-m/rad) observed in Fig. 22, that of the third appears to be about twice the observed (4,500 kN-m/rad). Therefore, with the same stiffness matrix, only the mode shapes were revised by adopting the measured mode shapes at the time t = 3.05 sec and t = 5.13 sec, as shown in Table 4.

Though the component corresponding to u_y in the mode vector could not be obtained from the measured mode shape in Table 4, the term containing u_y in eq. (3) was ignored because the absolute value of u_y and the constant, 419, are considered to be small when compared to those of u_x. Then, the values of torsional stiffness so calculated by using the measured mode vectors are 1,251 kN-m/rad and 4,072 kN-m/rad, for the second and third modes, respectively. These values are much more similar to those observed in tests.

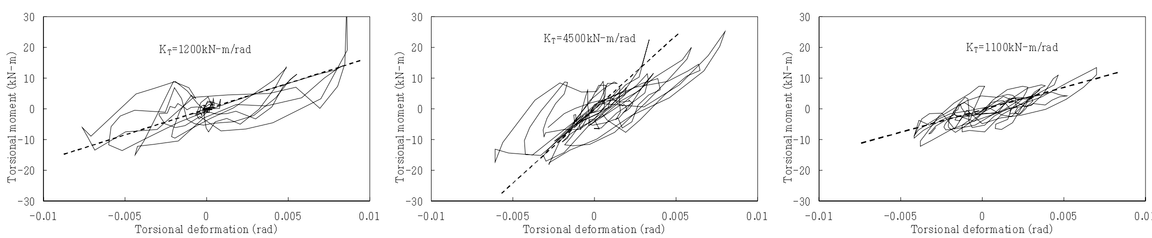

(a) 2 ~ 4 sec **(b) 4 ~ 6sec** **(c) 6 ~ 8sec**

Fig. 22 Variation of torsional stiffness (Model 3: Taft080)

Table 4 Mass matrix, stiffness matrix, mode vector for one-story model

D.O.F	Mass matrix (kN-sec²/mm)	Stiffness matrix (kN/mm)	Calculated mode vector	Measured mode shape: Second mode	Measured mode shape: Third mode
u_x u_y u_θ	$\begin{pmatrix} 0.0082 & 0 & 0 \\ 0 & 0.0082 & 0 \\ 0 & 0 & 1{,}583 \end{pmatrix}$	$\begin{pmatrix} 2{,}237 & 0 & 8{,}411 \\ 0 & 6.0 & -419 \\ 8{,}411 & -419 & 6{,}338{,}747 \end{pmatrix}$	$\begin{pmatrix} -508 & -583 & 333 \\ 2{,}208 & -216 & -101 \\ 1.0 & 1.0 & 1.0 \end{pmatrix}$	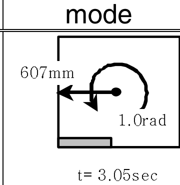	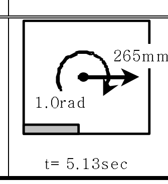

Base Shear and Torsional Moment (BST)

De la llera and Chopra [11] suggested use of the base shear-torque diagram (BST diagram) to conveniently observe and control the mode of vibration and failure. By assuming the elasto-plastic model in the relationship between the bent base shear and the drift at the level of transfer floor, as shown in Fig. 14 (c) for the three bents in the direction of earthquake excitation, and that the relations in the three bents perpendicular to the direction of excitation be the same as that of the flexible bent in the direction of excitation, BST diagram for the model is drawn in Fig. 23 (a). The outer solid line is the BST diagram which takes into account the contribution by the transverse bents while the inner dotted line is the one which does not. The implication of the contour in the BST diagram can be explained as follows: 1) The lines 1-2 and 5-6 mean that the bents parallel to the excitation have all yielded in the negative and positive direction, respectively, while the transverse bents remain elastic. 2) The lines 3-4 and 7-8 mean that all the perimeter bents yielded clockwise and counterclockwise, respectively, with the central bent in the direction of excitation being elastic. And, 3) the lines 2-3 and 6-7 mean that all the bents except the stiff bent have yielded, while the lines 8-1 and 4-5 imply that all the bents except the flexible bent in the direction of excitation yielded.

The ratio of the torsional moment to the base shear in each mode of vibration can be obtained by using the vectors of the corresponding mode shape. The ratio (M/V) for the second mode is 0.335 whereas that for the third mode is –0.576, if the mode shapes by analysis as given in Table 4 are used. If these two relations are plotted as lines anchored at the point (0,0), then the failure mode can be found at the 4 intersecting points. When the second mode governs, one of the failure or yielding modes is shown by the figure beside the point A in Fig. 23 (a). The shear in the stiff bent at this state is 12 kN, and therefore the total base shear will be 32 kN. This means that, under the coupled translational and torsional mode, only a small portion out of the whole capacity (70 kN) can be mobilized due to the coupling.

The hysteretic curves between the base shear and the torsional moment under Taft030 are superposed in Fig. 23 (a). It can be found that the model responded almost elastically under test and the predominant mode of vibration is the second mode. The hysteretic curves during t = 3 sec ~ 4 sec under Taft080 reveal the trend of the second mode as shown in Fig. 23 (b), but change this to that of the third mode during t = 4 sec ~ 6 sec as shown in Fig. 23 (c). Fig. 23 (b) shows that the total base shear (32 kN) and the state of bent shear forces at the time of failure turn out to be similar to the expected in Fig. 23 (a). The observations on Fig. 23 (c) are: (1) there remain relatively large residual base shears at the time when the torsional moments become zero, and (2) the magnitude of torsion is far less than the maximum torsional capacity. With these observations, it is apparent that the possibility of the occurrence of failure depicted by points C and D in Fig. 23 (a) is remote, while the possibility of failure, in which the base shear varies with the maximum torque being modest as shown in Fig. 23 (c), is very high.

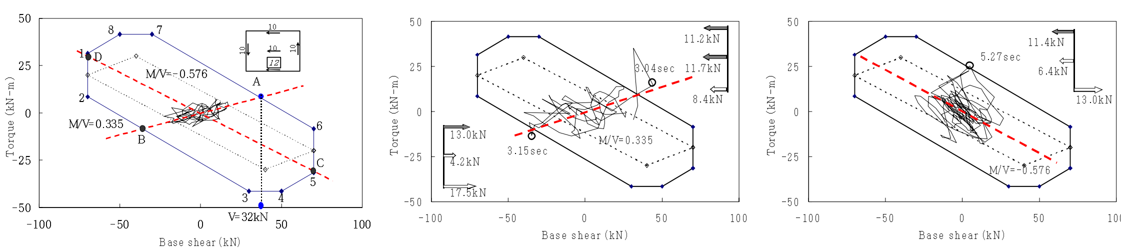

(a) Taft030 **(b) 3 ~ 4 sec (Taft080)** **(c) 4 ~ 6 sec (Taft080)**

Fig. 23 Relation between base shear and torsional moment

Behavior of wall

The time histories of the rotations of the shear wall at the level of the second floor (θ_{Wall}), that at the level of transfer floor (θ_2), and the uplift rotation at the level of the base (θ_{up}) under Taft080 are shown in Fig. 24. It is interesting to note: (1) the uplift rotation (θ_{up}), overturning deformation (θ_2) and wall rotation (θ_{Wall}) are always in phase during the excitation in Model 2. (2) While the uplift rotation is always in phase with the overturning deformation (θ_2), the wall rotation at the level of the second floor (θ_{Wall}) is in the same phase with the overturning rotation (θ_2) during the vibration of the second mode, but in the opposite phase during the vibration of the third mode in Model 3.

The fact that the rotations, θ_{Wall} and θ_2, and also θ_{Wall} and θ_{up}, have the opposite directions during the vibration of the third mode in Fig. 24 (b), means that there exist points of inflection in the shear wall at the first and second stories.

Fig. 25 (a) and (b) show the hysteretic relations between the rotation of the wall at the level of the second floor and the value of the wall base shear (V) multiplied by the height of the first story (h) under Taft080 for Model 2 and Model 3, respectively. Model 2 shows the response of single curvature over the whole duration whereas Model 3 reveals a mass of complicated curves. However, when this behavior of Model 3 is closely investigated with separate time intervals as shown in Fig. 26, the trend appears to be clear. During the interval t = 2 ~ 4 sec, the wall shows the behavior of single curvature, but it changes to that of double curvature during the interval t = 4 ~ 6 sec, and then returns to the mixed behavior of single and double curvatures during t = 6 ~ 8sec. This phenomenon reapproves the existence of inflection point in the shear wall at the first story in Model 3 subjected to the third mode from the view point of member forces.

The time histories of the elongation of exterior column of wall (Δ_{col}) and the torsional deformation (θ_3) are shown in Fig. 27. It is interesting to note that the torsional deformation (θ_3) is exactly in phase with, almost proportional to, the elongation of exterior columns at the level of the second floor (Δ_{col}). This

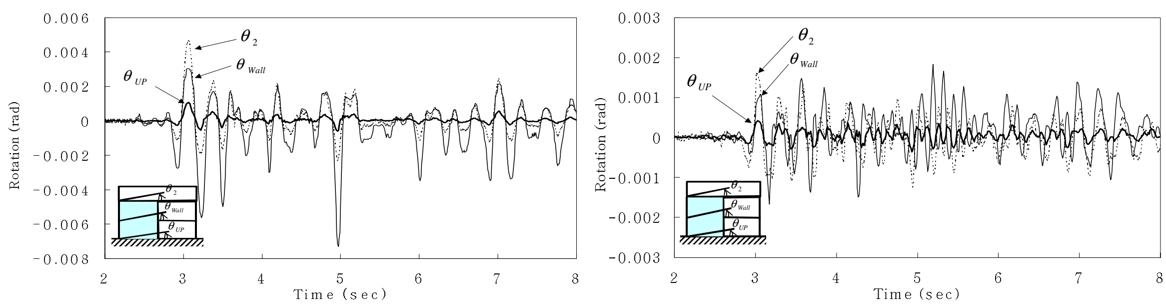

(a) Model 2 **(b) Model 3**

Fig. 24 Rotations of wall at transfer floor, 2nd floor, and base (Taft080)

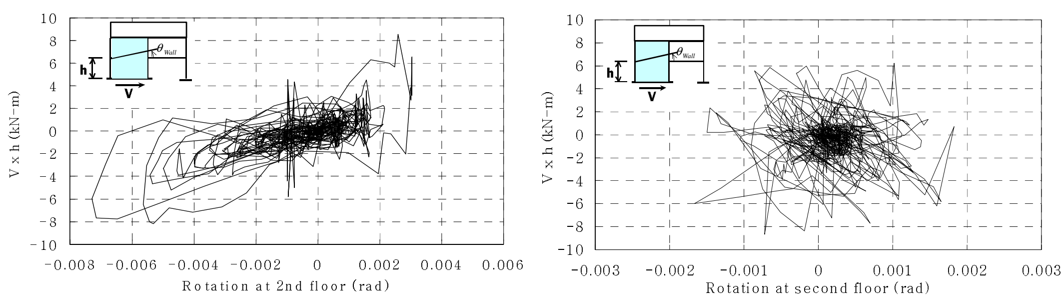

(a) Model 2 **(b) Model 3**

Fig. 25 Relation between rotation at second floor and Vh (Taft080)

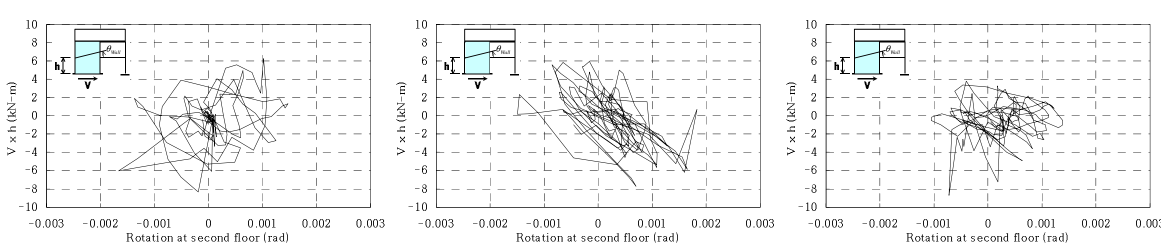

(a) 2 ~ 4sec **(b) 4 ~ 6sec** **(c) 6 ~ 8sec**

Fig. 26 Variation of the governing modes in Model 3 (Taft080)

phenomenon clearly reveals that the torsional behavior in plan is closely related to the elongation of columns through warping and, therefore, to the rotation of the shear wall in elevation. In other words, the warping behavior due to the torsion influences the distribution of moment and curvature (rotation) along the shear wall at bottom stories.

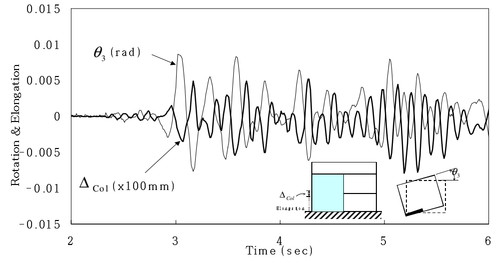

Fig. 27 Elongation of boundary column of wall and torsional deformation

Failure mode

Fig. 28 (a) and (b) show the crack patterns in the piloti portions of Model 1 and 2. it is clear that the columns in Model 1 had experienced high compressive and tensile forces under the Taft080. That is, the tensile and flexural failure can be noticed from many horizontal cracks at the top of the exterior column. The very high compressive forces in the exterior column caused the spalling of concrete and the buckling of longitudinal bars just beneath the load cell in both models. Fig. 28 (c) shows the crack patterns in Model 3. The flexible bent frame reveals the severe damage, such as cracks in beams at the face of columns, in the interior beam-column joint, and the crushing of concrete beneath the load cells. Generally, the exterior columns show many horizontal cracks due to the large overturning moment.

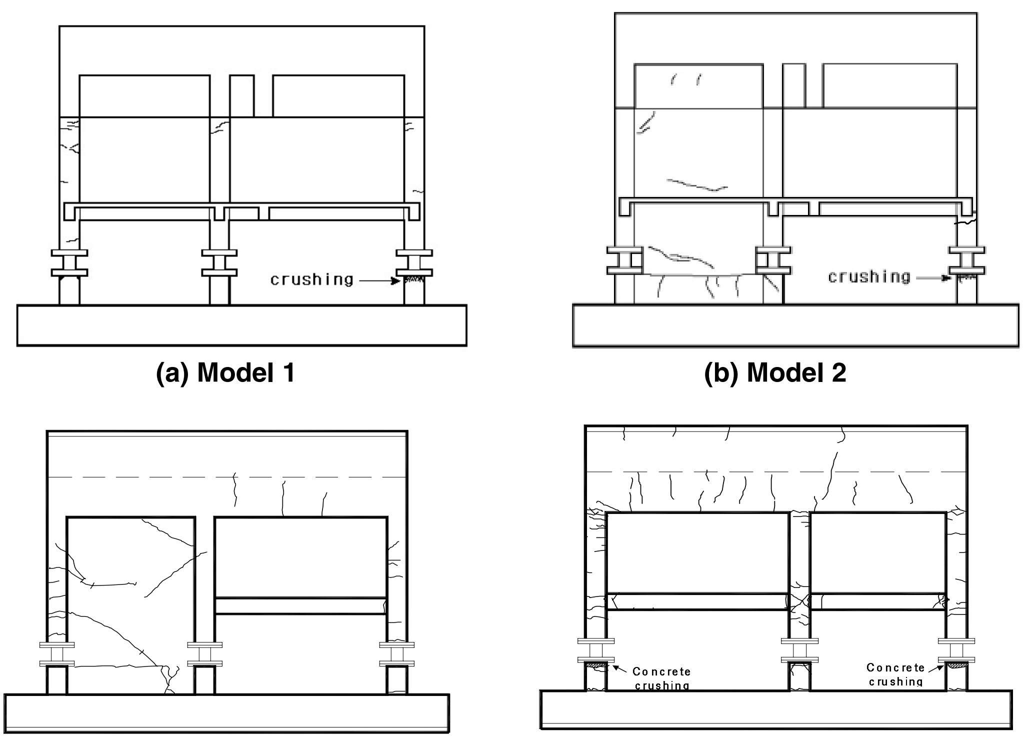

(a) Model 1 **(b) Model 2**

(c) Model 3 (Stiff frame) **(d) Model 3 (Flexible frame)**

Fig. 28 Final crack patterns

CONCLUSIONS

The following conclusions can be drawn based on the above observations:
1) The existence of shear wall reduces remarkably shear deformation at the lower frame, but has almost a negligible effect on the reduction of the overturning deformation, base shear, and OTM.
2) As the earthquake intensity increases, the structures with symmetric plan experienced the shift of rotating axis (rocking behavior) due to OTM. The model with torsional irregularity shows the uni-directional OTM transverse to the direction of excitations. The effects of two orthogonal OTM's and torsional moment complicate the distribution of axial forces in columns, which need further analytical research in the future.
3) The value of torsional stiffness varies depending on the governing mode of vibrations. A higher mode of vibration induces larger torsional stiffness. And, hysteretic curves and the strength diagram between base shear and torque clearly reveal the most probable mode of vibration leading to failure.

ACKNOWLEDGEMENT

The experimental part of the research was supported by the Ministry of Construction and Transportation, the Republic of Korea, Korea National Housing Corp., and several private companies including Ssangyong Engineering & Construction Co. Ltd., Kolon Engineering & Construction Co. Ltd., and Hyungsang Structural Engineering Co. Ltd. The interpretation part of the research was conducted during the sabbatical leave of the first author granted by Korea University, and also through the six-month program of exchanging scholar co-granted by Korea Science and Engineering Foundation (KOSEF) and Japan Society for the Promotion of Science (JSPS) in 2002.

REFERENCES

1. Lee, H.S. et al., "A Review of Design Practice for the Hybrid Structures with Upper Shear-wall and Lower-Frame Systems." Proceeding of Spring Conference, Korea Concrete Institute, 1999; 11(1): 223-228 (in Korean).
2. Korea Concrete Institute, "Design Code for Concrete Structure." Korea Concrete Institute, Seoul, 2000 (in Korean).
3. Architecture Institute of Korea, "Standard Design Loads for Buildings." Architecture Institute of Korea, 2000 (in Korean).
4. Hosoya, H., "Shaking Table Tests of Three-Dimensional Scale Models of Reinforced Concrete High-Rise Frame Structures with Wall Columns." ACI Structural Journal 1995; 92(6): 765-780.
5. Lee, H.S. et al., "Shaking table tests of a high RC bearing-wall structure with bottom piloti stories." Journal of Asian Architecture and Building Engineering 2002; 1(1): 47-54.
6. Lee, H.S. et al., "Effect of shear walls on seismic performance of piloti-type high-rise RC bearing-wall structures." Structural Engineers World Congress 2002, Yokohama, Japan, 2002.
7. Chopra AK. "Dynamics of structures." Prentice-Hall, New Jersey, 2002.
8. International Code Council (ICC). "International Building Code." International Code Council, 2000.
9. Paulay T and Priestley MJN. "Seismic design of reinforced concrete and masonry buildings." John Wiley & Sons, New York, 1992.
10. International Council of Building Officials (ICBO). "Uniform Building Code." International Council of Building Officials. Whittier, CA, 1997.
11. De la llera JC and Chopra AK., "Understanding the inelastic seismic behaviour of asymmetric-plan buildings." Earthquake Engineering and Structural Dynamics 1995; 24(4): pp. 549-572.